Table 2 Segmental PET/CT and LGE data

	Extent of LGE (%)					
	Control (n=372)	0–25 (n=190)	25–50 (n=83)	50–75 (n=54)	≥75 (n=37)	p value (ANOVA)
ATF	0.76±0.09	0.77±0.09	0.75±0.11	0.73±0.08	0.68±0.11**	<0.001
PTF (g ml^{-1})	0.72±0.08	0.72±0.09	0.70±0.09	0.60±0.08**	0.51±0.12***	<0.001
PTI	0.91±0.08	0.89±0.09	0.89±0.09	0.77±0.10**	0.70±0.16***	<0.001
MBF (ml g^{-1} min^{-1})	1.02±0.30	0.91±0.26*	0.85±0.30*	0.83±0.24*	0.67±0.30**	<0.001

*p<0.05 vs. control; **p<0.05 vs. control, 0–25 % LGE and 25–50 % LGE; ***p<0.05 vs. control, 0–25 % LGE, 25–50 % LGE and 50–75 % LGE.

PET/CT and CMR parameters

PET/CT and CMR data are summarized in Table 2. There was a gradual decrease in PTF, PTI and MBF values with increasing degree of LGE on CMR images (p<0.001 by ANOVA). ATF values remained relatively constant, except for a significant decrease in the (near) transmurally enhanced segments (p<0.001 by ANOVA).

Predictive values for viability

Figure 2 shows a concordant pattern between parametric PTF, PTI and LGE CMR images in a patient with ischaemic cardiomyopathy after an anterior myocardial infarction.

Using CMR as a reference, 91 of 364 (25 %) segments showing some degree of LGE were judged to be nonviable (LGE >50 %). As shown in Fig. 3, the values of PTF and PTI for predicting myocardial viability in all 736 segments were comparable (AUC 0.87, CI 0.83–0.90, and 0.86, CI 0.82–0.91, respectively, p=0.541). MBF was able to predict myocardial viability with less accurate (AUC 0.69, CI 0.63–0.75, p<0.001). Optimal cut-off values of PTF, PTI and MBF for predicting (near) transmural LGE on CMR were 0.69 g ml^{-1}, 0.80, and 0.78 ml min^{-1} g^{-1} with sensitivities of 69 %, 91 % and 72 %, and specificities of 87 %, 73 % and 56 %, respectively. Figure 4 shows an example of a patient with a nontransmural scar and a corresponding relatively high PTI.

Discussion

The present study was conducted to validate the use of a parametric myocardial viability imaging technique using [^{15}O]H_2O PET/CT in patients with ischaemic heart disease. Viability assessed using parametric PTF and PTI imaging was in good agreement with that assessed using LGE CMR. Furthermore, these images and myocardial perfusion

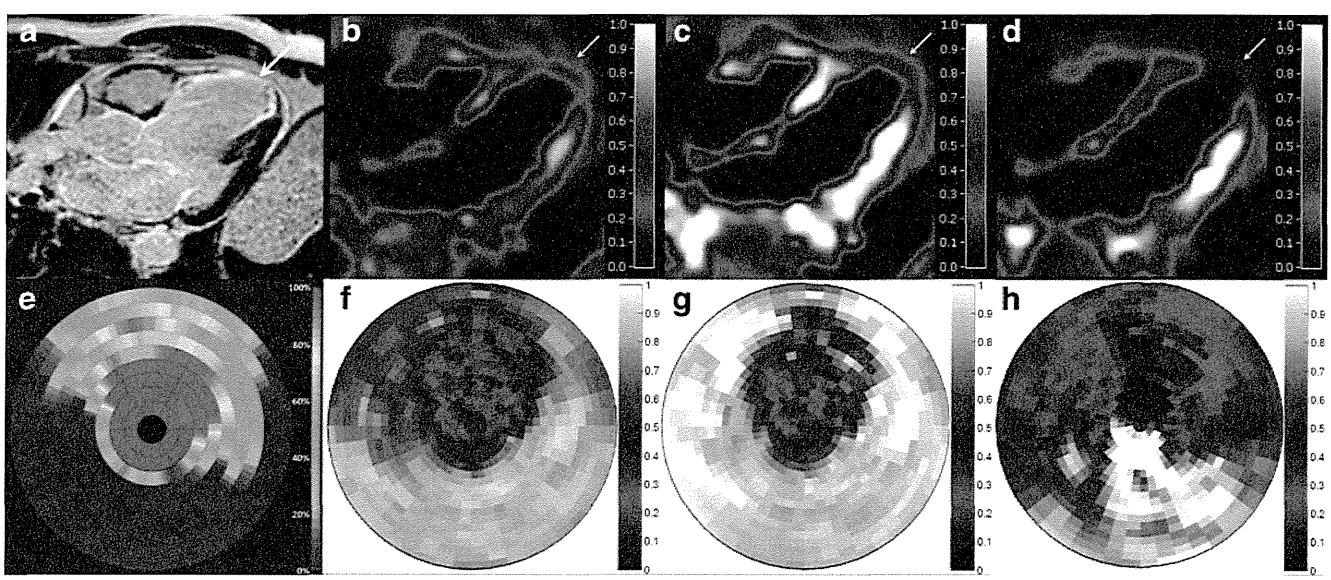

Fig. 2 Long axis images (**a**–**d**) and polar maps (**e**–**h**) in a patient with an anterior myocardial infarction: **a**, **e** CMR with LGE (*arrow*, % transmurality); **b**, **f** PTF (g ml^{-1}); **c**, **g** PTI; **d**, **h** MBF (ml g^{-1} min^{-1})

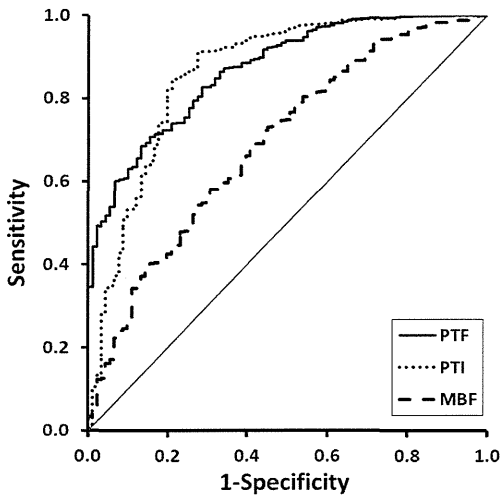

Fig. 3 Receiver operator characteristics curves for the abilities of PTF, PTI and MBF to differentiate between viable and nonviable segments based on late gadolinium enhancement

imaging are obtained simultaneously allowing both myocardial viability and ischaemia to be evaluated in a single scanning session.

$[^{15}O]H_2O$ is generally considered to be the gold standard for absolute quantification of myocardial perfusion in vivo [10, 18, 19]. Apart from MBF, $[^{15}O]H_2O$ also provides estimates of the extent of myocardium within a ROI that is able to exchange water rapidly, i.e. PTF. Subsequently, PTF can be corrected for partial volume effects by dividing it by its anatomical counterpart ATF, resulting in PTI [5]. It has been shown that both PTF and PTI can identify myocardial scarring and thus can act as markers of viability [6]. Only recently, however, a method has been developed that enables generation parametric ATF, PTF and PTI images from a single $[^{15}O]H_2O$ PET/CT scan [8]. This obviates the need for a separate $[^{15}O]CO$ blood volume scan. In addition, the traditional (long) transmission scan can be replaced by a (rapid) low-dose CT scan, thereby shortening the total scanning time substantially. Now that the method has been shown to produce high-quality parametric images, its implementation into clinical practice needs investigation.

Using the described parametric imaging approach, the present study demonstrated that ATF was relatively constant independent of tissue characteristics of the myocardium. Only in (near) transmurally infarcted segments was ATF significantly reduced, most likely due to wall thinning, as ATF is prone to partial volume effects. In contrast, PTF and PTI progressively decreased with increasing extent of scarring, as shown by LGE CMR. These results are in line with those of previous studies in which reductions in both PTF and PTI were observed in nonviable scarred myocardium [6]. PTI in control segments appeared to be somewhat lower than the expected value of unity for normal segments (0.91 ± 0.08). This phenomenon has previously been observed in cardiomyopathy in both animal experiments and human studies [6, 20]. Slight misalignment between PET and CMR segments may have occurred to additionally account for this reduction in PTI. Furthermore, the presence of interstitial fibrosis in dilated cardiomyopathy may also explain this reduction in 'normal' segments that remains undetected on LGE CMR [21, 22].

Taking LGE as a reference, the optimal cut-off values for discriminating between viable and nonviable myocardium were 0.69 g ml^{-1} and 0.80 for PTF and PTI, respectively. AUC analysis revealed that the diagnostic accuracies with the two PET parameters were comparable. This suggests that the use of parametric PTF alone may suffice to assess viability. Although this would reduce the data processing time, it would not affect the scanning protocol, as for both parameters a dynamic $[^{15}O]H_2O$ PET scan in combination with a low-dose CT scan are required. In addition, the sensitivity of PTI exceeded that of PTF (91 % and 68 %, respectively), whereas for specificity the opposite pattern was observed (73 % and 78 %, respectively). Although further study is need to determine the cause of this discrepancy, as a potential clinical marker of viability PTI may be favoured over PTF to reduce false-negative findings in patients who might benefit from revascularization. It is of interest to note that, compared to PTF and PTI, MBF performed relatively poorly in distinguishing viable from nonviable tissue, rendering it less suitable for viability imaging. Previous studies have indicated that the optimal cut-off value for PTI is in the range 0.7–0.9. The threshold observed in the present study corresponds with that range.

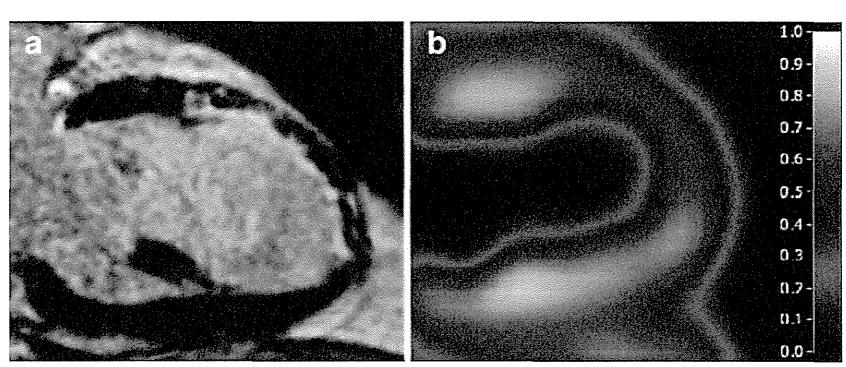

Fig. 4 Long axis images in a patient with a nontransmural anterior myocardial infarction: **a** CMR with LGE; **b** PTI

LGE was used as a surrogate end-point of myocardial viability instead of functional recovery of dysfunctional myocardium after revascularization. LGE has been shown to be a good, but not perfect, marker of myocardial viability [16, 17]. Therefore, the results should be interpreted with caution, and more studies are warranted to establish the value of parametric PTI as a viability marker.

Conclusion

PTF and PTI, obtained from a single [^{15}O]H_2O PET/CT scan, can be used as markers of myocardial viability in patients with coronary artery disease.

Acknowledgments This research was performed within the framework of CTMM, the Center for Translational Molecular Medicine (www.ctmm.nl), project COHFAR (grant 01 C-203), and was supported by The Netherlands Heart Foundation.

References

1. Wijns W, Vatner SF, Camici PG. Hibernating myocardium. N Engl J Med. 1998;339:173–81.
2. Yamamoto Y, de Silva R, Rhodes CG, Araujo LI, Iida H, Rechavia E, et al. A new strategy for the assessment of viable myocardium and regional myocardial blood flow using 15O-water and dynamic positron emission tomography. Circulation. 1992;86:167–78.
3. de Silva R, Yamamoto Y, Rhodes CG, Iida H, Nihoyannopoulos P, Davies GJ, et al. Preoperative prediction of the outcome of coronary revascularization using positron emission tomography. Circulation. 1992;86:1738–42.
4. Iida H, Tamura Y, Kitamura K, Bloomfield PM, Eberl S, Ono Y. Histochemical correlates of (15)O-water-perfusable tissue fraction in experimental canine studies of old myocardial infarction. J Nucl Med. 2000;41:1737–45.
5. Itoh H, Namura M, Seki H, Asai T, Tsuchiya T, Uenishi H, et al. Perfusable tissue index obtained by positron emission tomography as a marker of myocardial viability in patients with ischemic ventricular dysfunction. Circ J. 2002;66:341–4.
6. Knaapen P, Boellaard R, Götte MJ, van der Weerdt AP, Visser CA, Lammertsma AA, et al. The perfusable tissue index: a marker of myocardial viability. J Nucl Cardiol. 2003;10:684–91.
7. Knaapen P, Bondarenko O, Beek AM, Götte MJ, Boellaard R, van der Weerdt AP, et al. Impact of scar on water-perfusable tissue index in chronic ischemic heart disease: evaluation with PET and contrast-enhanced MRI. Mol Imaging Biol. 2006;8:245–51.
8. Harms HJ, de Haan S, Knaapen P, Allaart CP, Lammertsma AA, Lubberink M. Parametric images of myocardial viability using a single 15O-H2O PET/CT scan. J Nucl Med. 2011;52:745–9.
9. Kajander S, Joutsiniemi E, Saraste M, Pietilä M, Ukkonen H, Saraste A, et al. Cardiac positron emission tomography/computed tomography imaging accurately detects anatomically and functionally significant coronary artery disease. Circulation. 2010;122:603–13.
10. Knaapen P, de Haan S, Hoekstra OS, Halbmeijer R, Appelman YE, Groothuis JG, et al. Cardiac PET-CT: advanced hybrid imaging for the detection of coronary artery disease. Neth Heart J. 2010;18:90–8.
11. Boellaard R, Knaapen P, Rijbroek A, Luurtsema GJ, Lammertsma AA. Evaluation of basis function and linear least squares methods for generating parametric blood flow images using 15O-water and positron emission tomography. Mol Imaging Biol. 2005;7:273–85.
12. Harms HJ, Knaapen P, de Haan S, Halbmeijer R, Lammertsma AA, Lubberink M. Automatic generation of absolute myocardial blood flow images using [(15)O]H(2)O and a clinical PET/CT scanner. Eur J Nucl Med Mol Imaging. 2011;38:930–9.
13. Watabe H, Jino H, Kawachi N, Teramoto N, Hayashi T, Ohta Y, et al. Parametric imaging of myocardial blood flow with 15O-water and PET using the basis function method. J Nucl Med. 2005;46:1219–24.
14. Hermansen F, Rosen SD, Fath-Ordoubadi F, Kooner JS, Clark JC, Camici PG, et al. Measurement of myocardial blood flow with oxygen-15 labelled water: comparison of different administration protocols. Eur J Nucl Med. 1998;25:751–9.
15. Austen WG, Edwards JE, Frye RL, Gensini GG, Gott VL, Griffith LS, et al. A reporting system on patients evaluated for coronary artery disease. Report of the Ad Hoc Committee for Grading of Coronary Artery Disease, Council on Cardiovascular Surgery, American Heart Association. Circulation. 1975;51:5–40.
16. Kühl HP, Lipke CS, Krombach GA, Katoh M, Battenberg TF, Nowak B, et al. Assessment of reversible myocardial dysfunction in chronic ischaemic heart disease: comparison of contrast-enhanced cardiovascular magnetic resonance and a combined positron emission tomography-single photon emission computed tomography imaging protocol. Eur Heart J. 2006;27:846–53.
17. Wu YW, Tadamura E, Yamamuro M, Kanao S, Marui A, Tanabara K, et al. Comparison of contrast-enhanced MRI with (18)F-FDG PET/201Tl SPECT in dysfunctional myocardium: relation to early functional outcome after surgical revascularization in chronic ischemic heart disease. J Nucl Med. 2007;48:1096–103.
18. Bol A, Melin JA, Vanoverschelde JL, Baudhuin T, Vogelaers D, De Pauw M, et al. Direct comparison of [13N]ammonia and [15O] water estimates of perfusion with quantification of regional myocardial blood flow by microspheres. Circulation. 1993;87:512–25.
19. Iida H, Kanno I, Takahashi A, Miura S, Murakami M, Takahashi K, et al. Measurement of absolute myocardial blood flow with H215O and dynamic positron-emission tomography. Strategy for quantification in relation to the partial-volume effect. Circulation. 1988;78:104–15.
20. Teramoto N, Koshino K, Yokoyama I, Miyagawa S, Zeniya T, Hirano Y, et al. Experimental pig model of old myocardial infarction with long survival leading to chronic left ventricular dysfunction and remodeling as evaluated by PET. J Nucl Med. 2011;52:761–8.
21. Knaapen P, Götte MJ, Paulus WJ, Zwanenburg JJ, Dijkmans PA, Boellaard R, et al. Does myocardial fibrosis hinder contractile function and perfusion in idiopathic dilated cardiomyopathy? PET and MR imaging study. Radiology. 2006;240:380–8.
22. Iles L, Pfluger H, Phrommintikul A, Cherayath J, Aksit P, Gupta SN, et al. Evaluation of diffuse myocardial fibrosis in heart failure with cardiac magnetic resonance contrast-enhanced T1 mapping. J Am Coll Cardiol. 2008;52:1574–80.

Ann Nucl Med (2012) 26:644–655
DOI 10.1007/s12149-012-0631-2

ORIGINAL ARTICLE

F-18 fluorodeoxyglucose uptake and water-perfusable tissue fraction in assessment of myocardial viability

Hidehiro Iida · Ulla Ruotsalainen · Maija Mäki · Merja Haaparnata · Jörgen Bergman · Liisa-Maria Voipio-Pulkki · Pirjo Nuutila · Kazuhiro Koshino · Juhani Knuuti

Received: 8 November 2011 / Accepted: 18 June 2012 / Published online: 15 July 2012

Abstract
Objectives ^{15}O-water-perfusable tissue fraction (PTF) has been shown to be a potential index for assessing myocardial viability in PET, an alternative to ^{18}F-fluorodeoxyglucose (FDG). This study aimed to directly compare these two independent methods in assessing myocardial viability in patients with abnormal wall motion.
Methods PET study was performed on 16 patients with previous myocardial infarction, before coronary artery bypass graft operation (CABG). The protocol included a ^{15}O-carbonmonoxide static, a ^{15}O-water dynamic and an ^{18}F-FDG dynamic scan, during the euglycemic hyperinsulinemic clamp. Echocardiography was performed at the time of PET and 5–12 months after the CABG, and the wall motion recovery was evaluated on segmental and global bases. Consistency between PTF and ^{18}F-FDG was evaluated visually and also in a quantitative manner. Predictive values for the wall motion recovery were also compared between the two approaches.
Results The image quality of ^{18}F-FDG was superior to that of ^{15}O-water. The qualitative PTF showed significantly smaller defects than ^{18}F-FDG, and the quantitative PTF showed slightly greater values than ^{18}F-FDG in the infarcted region. The two methods were, however, consistent visually and also quantitatively. The predictive values of the wall motion recovery were almost equal between the two approaches. The absolute ^{18}F-FDG uptake was varied in normal segments, and predictive values for the wall motion recovery by the absolute ^{18}F-FDG was less (accuracy: 80 %) compared with those by the relative ^{18}F-FDG (accuracy: 87 %) and the quantitative PTF (accuracy: 89 %).
Conclusion Despite the small sample size, PTF appears to give consistent results with the ^{18}F-FDG approach, and might be an alternative viability assessment.

Keywords Myocardial viability · Chronic myocardial infarction · ^{18}F-FDG · Water perfusable tissue fraction · Positron emission tomography

H. Iida · M. Haaparnata · J. Bergman · P. Nuutila · J. Knuuti
Turku PET Center, Turku University Central Hospital, 20520 Turku, Finland

H. Iida (✉) · K. Koshino
Department of Investigative Radiology, National Cerebral and Cardiovascular Center Research Institute, 5-7-1 Fujishiro-dai, Suita, Osaka 565-8565, Japan
e-mail: iida@ri.ncvc.go.jp

U. Ruotsalainen · M. Mäki · L.-M. Voipio-Pulkki
Department of Nuclear Medicine, Turku University Central Hospital, 20520 Turku, Finland

U. Ruotsalainen
Department of Signal processing, Tampere University of Technology, 33720 Tampere, Finland

L.-M. Voipio-Pulkki
Departments of Medicine, Helsinki University Central Hospital, 00029 Helsinki, Finland

Introduction

Successful coronary reperfusion by thrombolysis, angioplasty, or bypass graft surgery is often associated with improvement of myocardial contractile function in patients with coronary disease, suggesting the presence of dysfunctional but viable myocardium within the area of abnormal wall motion [1–3]. Several techniques have been proposed for detecting the reversibly injured myocardium in the clinical setting including single photon emission computed tomography (SPECT) with ^{201}Tl or ^{99m}Tc-MIBI,

echocardiography during dobutamine stimulation, and flow-metabolism imaging with positron emission tomography (PET). Of these, ^{18}F-FDG and PET [4–7] have been considered to be the gold standard. Commonly, increased ^{18}F-FDG uptake relative to blood flow has been judged as a sign of preserved myocardial viability. The advantages of ^{18}F-FDG PET include the good quality of the images and high accumulation of the tracer into dysfunctional but viable myocardium. Image quality can further be improved by performing the studies during euglycemic hyperinsulinemic conditions [8]. It is suggested that the maximized ^{18}F-FDG uptake makes the tracer distribution proportional to the amount of viable myocardium.

^{18}F-FDG is on the other hand a marker of glucose uptake, which depends on a number of physiologic factors such as myocardial work load, metabolic conditions of the subject and hormones, suggesting limitations of utilizing ^{18}F-FDG PET for the viability assessment. Indeed, it has been demonstrated that the normalized uptake of ^{18}F-FDG relative to a control region is more accurate in predicting wall motion recovery after coronary artery bypass graft surgery [9].

An alternative approach has been proposed, employing ^{15}O-labeled radiotracers [10–13]. This enables the direct measurement of the proportion of ^{15}O-water perfusable tissue that is capable of exchanging water rapidly. The water perfusable tissue fraction (PTF, g/ml) was defined as the fraction of the water-perfusable tissue within a given volume of region-of-interest (ROI), and is measured from the kinetic analysis on the ^{15}O-carbonmonoxide and ^{15}O-water data sets. Similarly, the perfusable tissue index (PTI) was defined as the proportion of the ^{15}O-water perfusable tissue within the total anatomical tissue that was measured from the transmission (tissue density) scan. These parametric values were originally assessed for given ROIs. A qualitative, myocardial distribution of radioactive water at a later phase reasonably corresponded to a relative PTF distribution [13], which was also shown to be consistent with the relative distribution of FDG accumulation in an experimental pig model of old myocardial infarction [14]. More recently, sophisticated computer programs have provided functional parametric images of quantitative PTF and PTI from a single dynamic PET image obtained following intravenous ^{15}O-water [15–17].

There can be tradeoffs between the ^{18}F-FDG and PTF (and PTI) approaches, in terms of the total study duration, radiation dose, cost of the procedure, image quality, sensitivity to various error sources, etc. There have, however, been no direct comparisons between ^{18}F-FDG and PTF in the assessment of myocardial viability in a clinical patient population. Against this background, we performed a head-to-head comparison between ^{18}F-FDG uptake and PTF in patients with chronic coronary artery disease who underwent revascularization. Consistency between ^{18}F-FDG and PTF studies was evaluated both visually and in a quantitative manner. Predictive value of wall motion recovery after successful revascularization therapy was also compared between the two measures.

Materials and methods

Subjects

The study group consisted of 16 patients (15 males and 1 female). In 10 of them, a myocardial infarction was diagnosed previously both by electrocardiographic and enzymatic criteria. In the other 6 patients, chronic left ventricular dysfunction and an occluded major coronary artery were detected but there were no confirmed data available on previous myocardial infarction. The patient characteristics are summarized in Table 1. All patients had stable, angiographically confirmed coronary artery disease and a permanent wall motion abnormality at rest. Three had diabetes mellitus, and three had heart failure. The interval between the acute event and the PET study was more than 5 months. All of them underwent coronary artery bypass grafting (CABG) after the PET imaging. There was no particular change in the patient's symptoms between the time of the PET study and the time of CABG. The study was approved by the Ethics Committee of the Turku University Central Hospital, Turku City, Finland [8/1993 § 153 (dated 19.10.1993)]. All studies were performed in accordance with the ethical standards laid down in the Declaration of Helsinki and subsequent guidelines at Turku University. Informed consent was given by each patient prior to his inclusion in the study. No subjects have any particular issues that might reveal their identity.

Study design

All patients underwent coronary angiography, radionuclide ventriculography, ^{201}Tl SPECT, echocardiography, and PET imaging before the CABG. The PET imaging included scans with ^{15}O-carbonmonoxide, ^{15}O-water and ^{18}F-FDG during euglycemic hyperinsulinemic clamp (see Fig. 1). Angiography was performed 9.1 ± 4.4 weeks before the PET study (all within 4 months). Echocardiography was performed on the same day of the PET imaging and repeated 5–12 months after CABG. Wall motion recovery was then evaluated for each dysfunctional segment in the preoperative study, and this was compared with the results from the PET and SPECT imaging. The consistency of different PET images was also evaluated.

Table 1 Patient characteristics

Patient #	Age	Weight (kg)	Duration of CAD (months)	NYHA	Heart failure	Medication	Time between angiogram and PET (weeks)	EF (%) Pre ope.	EF (%) Post ope.	HR	Systolic blood pressure (mmHg)	Diastolic blood pressure (mmHg)	Blood glucose (mmol/l)
1	41	85	5	2	N	Beta blocker, nitrate	8	25	19	67	105	67	5.33
2	56	87	216	2	N	Beta blocker, nitrate	12	24	19	71	120		5.48
3	64	80	17	3	Y		6	33	35	64	133	85	5.48
4	44	75	9	2	N	Beta blocker, nitrate	4	28	38	75	104	67	4.52
5	64	90	96	3	Y	Nitrate	8	49	55	55	136	83	4.41
6	44	105	9	2	N		12	56	31	65	140	90	5.24
7	65	98	72	3	N	Beta blocker, nitrate	8	48	61	59	146	85	4.91
8	55	89	6	2	N	Beta blocker, nitrate	12	30	57	62	130	78	4.84
9	61	81	5	2	N	Ca-antagonist, nitrate	16	54	42	90	150	80	4.52
10	69	67	69	2	N	Ca-antagonist, nitrate	16	69	60	54	112		4.98
11	52	82	24	3	Y	Nitrate	8	48	58	50	135		5.01
12	56	83	240	3	N	Beta blocker, nitrate	4	31	52	51	119		5
13	57	89	66	3	N	Beta blocker, nitrate	4	60	53	61	132		5.4
14	70	82	21	3	N	Ca-antagonist, nitrate	16	51	64	64	171		5.1
15	48	77	7	2	N	Beta blocker, nitrate	8	57	68	52	133		6.39
16	71	76	360	3	N	Ca-antagonist, nitrate	4	68	68	65	178		6.59
Mean ± SD	57 ± 10	84 ± 9	76.4 ± 105.	2.5 ± 0.5			9.1 ± 4.4	46 ± 15	49 ± 16	62.8 ± 10.2	134 ± 21	79 ± 8	5.2 ± 0.6

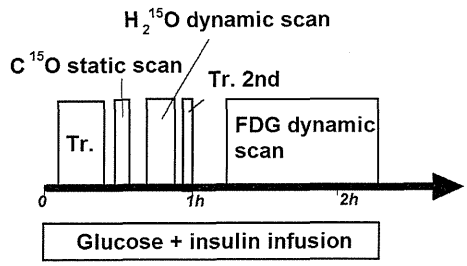

Fig. 1 Schematic diagram of the study protocol. *Tr* indicates the transmission scan. The second transmission scan was used to confirm that the patient did not move during the period

PET studies

PET scans were performed in 2D using an ECAT 931-08/12 scanner (CTI/Siemens Inc., Knoxville, Tenn.) [18]. This scanner enables 15 planes of data to be acquired in an axial field-of-view (FOV) of 10.5 cm. All emission and transmission sinograms were reconstructed with a Hanning filter with a cutoff frequency of 0.3. This resulted in a spatial resolution of 8.4 ± 0.7 mm full width at half maximum (FWHM) for the emission data and 7.7 ± 0.7 mm FWHM for the transmission data at the center of the FOV with the slice thickness of 6 mm.

All subjects fasted for at least 10 h before the PET scanning. Medications were continued as noted in Table 1. Patients lay supine on the scanner bed with their arms out of the FOV. Two catheters were placed, one in the antecubital vein for infusion of saline or glucose and insulin and ^{15}O-water and another in the radial vein of the contralateral hand that was warmed with air temperature of 70 °C for sampling of arterialized venous blood. During the whole study period, insulin was infused continuously as previously described to maintain the euglycemic hyperinsulinemic condition [8, 19, 20]. The rate of insulin infusion was 1 mU/kg/min. During hyperinsulinemia, euglycemia was maintained by infusing 20 % glucose. The rate of the glucose infusion was adjusted according to plasma glucose concentrations measured every 5–10 min from arterialized venous blood. Blood samples were taken at 30-min intervals for determination of insulin, free-fatty acid, and lactate concentrations.

A 20-min transmission scan was performed by exposure of the external ring source of ^{68}Ge. These data were used to correct for subsequent emission scans for photon absorption in the body, and to estimate the density distribution. After the transmission scan, the blood pool was imaged by inhalation of ^{15}O-labeled carbon monoxide. ^{15}O-carbon monoxide of approximately 3.7 GBq was administered for 2 min, and a 4 min, single frame emission acquisition was initiated at 2 min after the end of ^{15}O-carbonmonoxide inhalation. Venous blood samples were taken every 2 min during the scan, and the ^{15}O-carbonmonoxide concentration in whole blood was measured using a NaI well counter cross calibrated with the scanner.

After a 15-min period to allow for decay of ^{15}O-radioactivity to background levels, ^{15}O-water was infused and a dynamic PET scan was started using a previously reported protocol [21, 22]. Briefly, ^{15}O-water in 5-ml saline was infused into the antecubital vein at a constant rate for a period of 2 min. Total administration dose was 1.5 GBq. A 20 frame dynamic PET scan was started at the initiation of the infusion, and lasted for 6 min. The scan sequence consisted of 6 × 5 s, 6 × 15 s, and 8 × 30 s.

Metabolic imaging was then performed using ^{18}F-FDG. ^{18}F-FDG (240 ± 40 MBq) was infused intravenously over 2 min, and dynamic scanning was initiated at the start of infusion. This scan lasted for 60 min.

PET data analysis

All sinograms were corrected for tissue attenuation and reconstructed using a Filtered Back Projection method. Images were transferred to a Linux workstation, and further analyses were performed using the dedicated image analysis packages (Dr. View; Asahi-Kasei, Tokyo) and in-house software programs.

A blood volume image was calculated using the ^{15}O-carbonmonoxide emission data, in which the original image was divided by the average of the blood counts measured by the well counter. Images of extravascular density were created by subtracting images of the blood volume from the corresponding transmission images after conversion of the latter to tissue density.

The ^{15}O-water dynamic images were integrated over the period of ^{15}O-water administration, and the blood volume was subtracted as previously described [11, 23, 24]. These images (the build-up or BU phase images) were considered to qualitatively illustrate the regional distribution of myocardial blood flow. The ^{15}O-water dynamic images were also integrated over the washout period, and the blood volume was similarly subtracted. These images (the washout or WO phase images) were considered to correspond to the qualitative distribution of PTF [11, 13].

Quantitative values of MBF, PTF, and the arterial blood volume (V_a) were calculated for each segment (see below) according to the non-linear least squares fitting as validated previously [21]. The arterial input function was estimated from the left-ventricular time-activity curve, in which the limited recovery of left-ventricular chamber activity and the spillover from myocardium were corrected as reported previously [22, 25]. The adoption of PTF in this model has implications for the interpretation of MBF values, such that the measurement exclusively represents the mean regional flow to that mass of the tissue within the ROI that is

capable of exchanging water rapidly, i.e., that mass of tissue defined by PTF. This method provides regional blood flow only to the perfusable tissue, and has units of ml/min/g of perfusable tissue. In areas of myocardial infarction, this MBF represents the regional flow to the residual water-perfusable tissue. Another blood flow has also been calculated in this study as a product of MBF and PTF, which should represent the average blood flow to the volume of ROI (i.e., ml/min/ml of ROI). MBF_t is adopted to describe this parameter.

The absolute glucose consumption was calculated from the ^{18}F-FDG uptake for each segment by the graphical analysis [8]. The relative glucose or ^{18}F-FDG uptake, as well as the relative MBF images, was also calculated by normalizing the absolute quantitative values to the reference segment in each study. The reference segment was defined as the normal region (or closest to the normal) according to the findings of coronary angiography and echocardiography. The reference segment was the lateral wall in 14 studies, and anteroseptal segment in 2 studies.

Regions-of-interest

The myocardium was divided into eight segments according to the previously described criteria [8], namely the anterior basal, anterior, anteroseptal, lateral, inferoseptal, apical, inferior, and posteroseptal regions. Of these, the last seven segments were included in this analysis. ROIs were drawn for each of the seven segments manually on transaxial tomographic images of ^{18}F-FDG, and these ROIs were projected onto all other PET images.

Visual analysis

Consistency of the defect between different images was evaluated for the segments described above. The defect severity was graded visually into 4 levels and its consistency was compared at each segment. Approximately the following limits are used in the visual classification: normal: 100–75 % of reference, mild: 75–50 %, severe: 50–25 % and complete: <25 % of activity in the reference segment. Consistency of the defect was evaluated between the approaches, namely the ^{18}F-FDG image versus the ^{15}O-water washout phase image (i.e., the qualitative PTF), the ^{15}O-water build-up phase image (i.e., qualitative MBF) versus the ^{18}F-FDG image, and ^{15}O-water build-up phase image versus qualitative PTF image. The predictive values of the wall motion recovery after the revascularization were also compared among the approaches. In this analysis, the normal and mild defect segments were considered to be viable in all measures except for the qualitative PTF image, in which only the completely normal segment was assigned to be viable.

Quantitative analysis

The glucose consumption values (absolute and relative) were plotted as a function of the absolute MBF (MBF_t). The glucose consumption values were also compared with PTF.

Coronary angiography

All patients underwent selective coronary angiography by standard techniques. The cine tapes were analyzed by an experienced radiologist. A 50 % or greater reduction in the diameter in a major epicardial branch was considered significant.

Echocardiography

Two-dimensional echocardiography (Acuson 128XP/5, Acuson Inc or Aloka SSD 870, Aloka Inc) was performed on the same day as PET according to the semiquantitative method recommended by the American Society of Echocardiography Committee on Standards, but the segmental subdivision was modified to correspond to the PET studies [8]. Echocardiograms were analyzed by a blinded experienced physician. The results of individual prerevascularization and postrevascularization echocardiograms were ultimately verified by comparison of videotape recordings. Wall motion and thickening were scored according to the following scale: 1, normal; 2, hypokinetic wall motion with systolic thickening; 3, akinetic wall motion with no systolic thickening; and 4, dyskinetic wall motion and no systolic thickening.

After the revascularization, improvement of contractile function was diagnosed if systolic thickening (corresponding to a score of 1 or 2) became apparent in a segment that had been akinetic or dyskinetic or if normal motion was detected in a previous dysfunctional segment. Improvement in function was acknowledged only if it was apparent in a central area of the segment. Special attention was focused on the anteroseptal segments because postsurgical wall motion abnormalities are common in this area. Thus, appearance of postoperative anteroseptal hypokinesia was regarded as normal, and improvement was recognized only if systolic thickening became apparent in a previously akinetic or dyskinetic segment or if hypokinesia was normalized.

Radionuclide ventriculography

A gated, blood-pool, radionuclide ventriculography was performed in two views. Six hundred cycles (10 min) were collected after injection of 740 MBq of [^{99m}Tc]-labeled human serum albumin. The left anterior oblique view was

used for ejection fraction calculations. A Siemens-Orbiter gamma camera (Siemens Gammasonics, IL, USA) was used, and ejection fractions were calculated with the Gamma-11 program (Nuclear Diagnosis, Stockholm, Sweden).

Analytical procedures

Plasma glucose was determined in duplicate by the glucose oxidase method using an Analox GM7 (Analox Instruments LTD, London, England) glucose analyzer. Serum insulin was measured by radioimmunoassay kit (Pharmacia, Uppsala, Sweden).

Statistical analysis

Independent variables were compared by analysis of variance. All results are expressed as the mean and one standard deviation (SD). Sensitivity, specificity, and positive and negative predictive values of functional recovery were calculated for the measures. To test different threshold values in quantitative MBF, quantitative PTF and quantitative ^{18}F-FDG uptake in predicting functional recovery, the discriminant analysis of SAS statistical program was used (SAS Institute Inc., Cary, N.C.). Receiver operating characteristic (ROC) analysis was also applied for assessment of FDG uptake and PTF in differentiating functionally recovered from non-recovered segments.

Results

Hemodynamic and other parameters are summarized in Table 1. Plasma glucose and insulin concentrations were 6.0 ± 1.0 mmol/l and 12 ± 3 mU/l in the fasting state. During clamp serum insulin concentrations increased to 79 ± 19 mU/l. The plasma glucose concentrations were 5.2 ± 0.6 mmol/l during the PET studies (Table 1).

In total, 105 of the 112 segments in the 16 patients were included in the final analysis. The remaining 7 segments, mostly inferior, were excluded because they were out of FOV in the PET study. In the preoperative echocardiography, 48 segments had normal wall motion and of the 57 dysfunctional segments, 35 were hypokinetic, 17 were akinetic and 5 were dyskinetic. In the revascularization, 54 of the 57 dysfunctional segments were successfully revascularized.

In the postoperative echocardiography, 81 segments were normal, 6 were hypokinetic, 13 akinetic and 5 were dyskinetic. Thus, 34 (60 %) of the initially dysfunctional revascularized segments recovered (partially in one) and 20 (35 %) segments did not show functional improvement. In the 3 non-revascularized segments, wall motion was unchanged in two and worsened in one.

The preoperative ejection fraction was 45.7 ± 15.1 % (range from 24 to 69 %). Postoperatively the ejection fraction was slightly higher (49 ± 16 %) but the difference was not significant. However, the average wall motion score in echocardiography was significantly improved by revascularization (preoperatively 0.8 ± 0.9 vs. postoperatively 0.45 ± 0.9, $p = 0.001$). Furthermore, the number of segments recovered per patient was significantly associated with increased global left ventricular ejection fraction ($r = 0.65$, $p = 0.0065$).

Figure 2 shows examples of calculated images obtained from typical two studies, demonstrating the extravascular tissue density (D_{ev}), blood volume (V_B), ^{15}O-water image at a washout phase (i.e., the qualitative PTF), and ^{18}F-FDG uptake. In case 1, both PTF and FDG images showed a large defect in the anterior wall region, and these two images were considered to be consistent in all segments. No recovery of wall motion was detected after revascularization. In case 2, the anterior, anteroseptal and apical walls were akinetic. The FDG and PTF images indicated preserved myocardial viability in the former two segments but scar in the apex. After the revascularization, the anterior and anteroseptal segments were completely recovered but no change was detected in the apex.

Consistency of the defect scores defined by the visual analysis is summarized in Table 2. The qualitative MBF (^{15}O-water build-up phase images) and the qualitative PTF (^{15}O-water washout phase image) agreed in general with the ^{18}F-FDG images. It should, however, be noted that the qualitative PTF image tended to show less severe defects, and resulted in milder defect scores in 14 segments compared with the ^{18}F-FDG images. The ^{15}O-water images at the build-up phase (qualitative MBF) showed considerably larger defects as compared with PTF and ^{18}F-FDG.

The predictive values for the wall motion recovery resulted from the visual analysis are summarized in Table 3, in which the optimal defect score was determined so as to provide the best predictive accuracy for each parameter. The best sensitivity was obtained with ^{18}F-FDG, but the specificity of ^{18}F-FDG was slightly lower than that of qualitative PTF. The accuracy was almost equal between the ^{18}F-FDG and qualitative PTF image analysis.

Defects were frequently seen (12 of 15 cases) in the qualitative PTF images in the apical segment. Of these, 7 segments showed recovery, while the other 5 did not. All 3 segments assigned to be viable in the apex by the qualitative PTF image demonstrated recovery. In the ^{18}F-FDG image, 7 segments were assigned to be scar (out of 15) in the apex, of which 1 segment showed recovery. All segments (8 segments) assigned as normal or viable in the apical segment by the ^{18}F-FDG showed wall motion recovery.

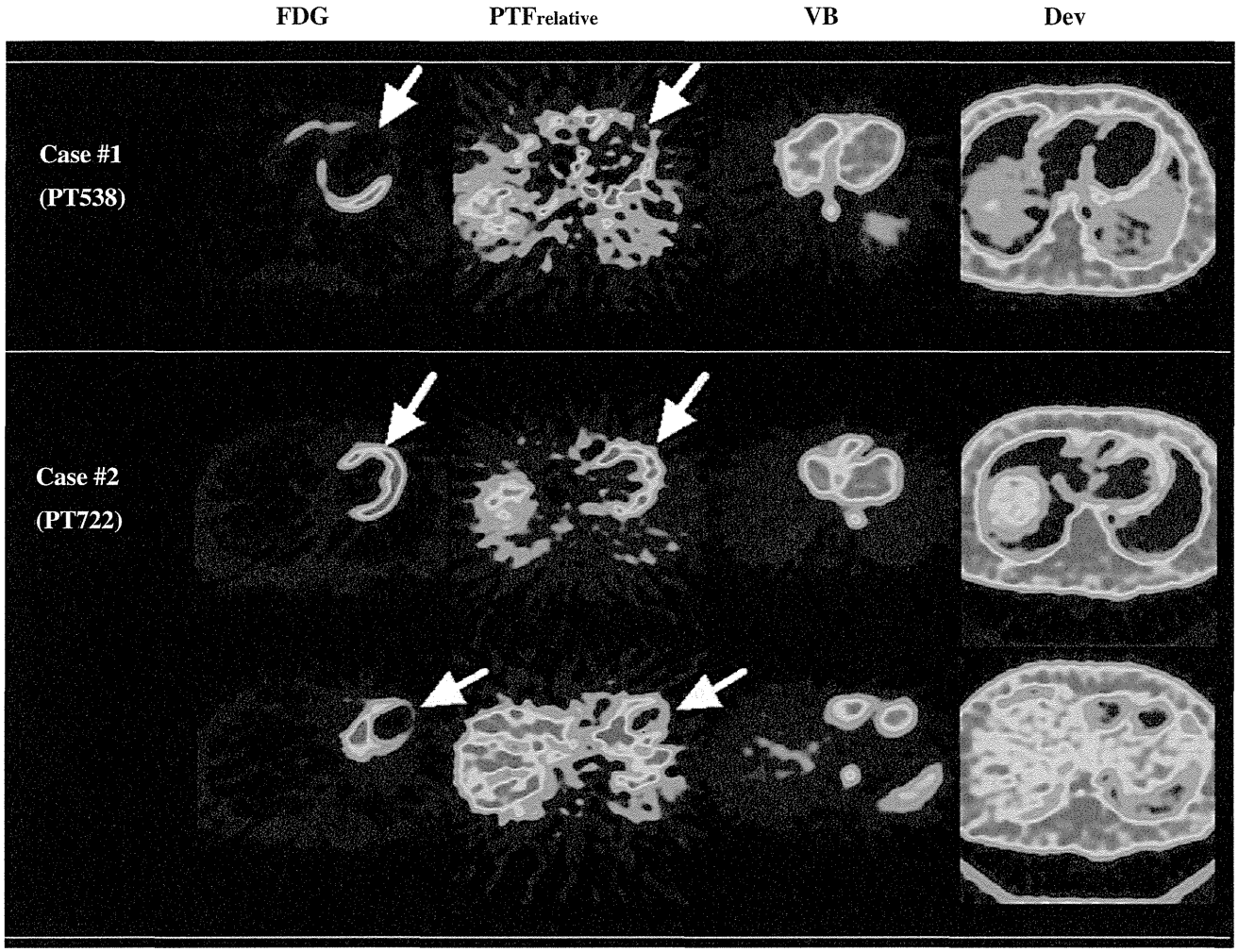

Fig. 2 Example images of extra-vascular tissue density (D_{ev}), the blood volume (V_B), ^{15}O-water washout phase (WO, or qualitative PTF), and ^{18}F-FDG uptake, obtained from 2 typical cases. In case 1, the wall motion was irreversible in the anterior wall segment (*arrow*, **a**), which was well predicted by both WO and FDG as complete defect. In case 2, wall motion was reduced in the anterior wall (*arrow*, **b**), but was not improved in the apex (*arrow*, **c**). These were also consistent with the findings in both WO and FDG. Image quality of ^{18}F-FDG was better than that of WO, but both images provided consistent results

Figure 3 shows the absolute and relative glucose uptake as a function of the absolute MBF, in which the flow per volume (i.e., the transmural flow) was adopted to the myocardial flow (i.e., the MBF estimated from the ^{15}O-water kinetic analysis was multiplied by PTF) [10, 11, 13]. The variability of absolute glucose uptake from patient to patient was larger as compared to relative values. Thus, the relation was diverged at the normal MBF range. On the other hand, the relative ^{18}F-FDG uptake which was normalized in each subject to the control segment was rather constant at the range: $MBF_t > 0.5$ ml/min/ml. The relative ^{18}F-FDG uptake showed a large variation at the range of MBF_t between 0.3 and 0.5 ml/min/ml, and was decreased linearly with the MBF_t for $MBF_t < 0.3$ ml/min/ml. There was no significant correlation between absolute glucose uptake and PTF, while a significant correlation was observed if the relative ^{18}F-FDG uptake was compared with PTF ($p < 0.001$) (Fig. 4).

Predictive values for the wall motion recovery resulted from the quantitative analysis are summarized in Table 4 and Fig. 5. The most accurate results were obtained using the limit values of 0.62 ml/min/g in MBF, 0.34 ml/min/ml in MBF_t, 0.51 g/ml in PTF, 34.4 mol/100 g/min in the absolute ^{18}F-FDG uptake and 67 % in the relative ^{18}F-FDG uptake. The positive predictive values obtained with the different variables were nearly equal among the variables. However, the absolute ^{18}F-FDG uptake and MBF showed clearly lower negative predictive values than relative ^{18}F-FDG uptake and PTF values. Figure 6 shows the results of ROC analysis for FDG uptake and PTF. The ROC analysis demonstrated greater area under the curve in relative rather than absolute values for both FDG and PTF. The area under

Table 2 Image consistency as evaluated by the defect score by visual analysis

FDG uptake vs. qualitative PTF or ^{15}O-water washout phase image						
FDG	PTF					
	0	1	2	3	Total	
0	73	1	2	0	76	
1	6	7	0	1	14	
2	0	4	1	0	5	
3	0	2	2	6	10	
Total	79	14	5	7	105	Concordance = 83 %
Qualitative MBF or ^{15}O-water build-up phase vs. FDG uptake						
MBF	FDG					
	0	1	2	3	Total	
0	65	3	0	1	69	
1	2	4	0	0	6	
2	8	4	3	2	17	
3	1	3	2	7	13	
Total	76	14	5	10	105	Concordance = 75 %
Qualitative MBF or ^{15}O-water build-up vs. qualitative PTF or ^{15}O-water washout phase						
MBF	PTF					
	0	1	2	3	Total	
0	68	0	0	1	69	
1	5	1	0	0	6	
2	6	8	3	0	17	
3	0	5	2	6	13	
Total	79	14	5	7	105	Concordance = 74 %

Table 3 Results of visual analysis in terms of evaluating wall motion recovery

Images	Sensitivity (%)	Specificity (%)	PPV (%)	NPV (%)	Accuracy (%)
FDG uptake	97	70	85	93	87
Qualitative MBF (^{15}O-water build-up)	82	75	90	60	80
Qualitative PTF (^{15}O-water washout)	88	85	91	81	87

Upper values correspond to only dysfunctional segments, and lower to total segments

the curve was slightly greater with PTF rather than relative FDG. Combination of FDG with MBF is of interest in terms of the improved accuracy in determining wall motion recovery. The best accuracy was obtained by the combination of relative ^{18}F-FDG uptake and relative MBF (Table 4).

There were 4 errors in PTF (out of 15) in the apical segment, in which PTF was below the threshold value (values ranged from 0.41 to 0.48 g/ml) and assigned not to be viable, although the wall motion was recovered or normal in the preoperative study. Similarly ^{18}F-FDG showed error in 3 apical segments, in which the values were below the threshold level, although the wall motion was normal or reversible.

Discussion

The present study demonstrated a direct comparison between the ^{18}F-FDG and PTF approaches in the assessment of myocardial viability in a clinical patient population. Despite the small number of subjects ($n = 16$), it was shown that the relative uptake of ^{18}F-FDG well correlated with the quantitative PTF. In the visual evaluation, although the image quality was superior with ^{18}F-FDG than the ^{15}O-water-based qualitative PTF images, the two images were consistent with each other. Furthermore, both images of relative ^{18}F-FDG uptake and PTF (as well as the qualitative washout phase images for ^{15}O-water) well predicted the wall motion recovery after successful revascularization in the dysfunctional segments. The area under the curve in the ROI analysis also demonstrated similar values between the relative FDG uptake and PTF. The accuracy appeared to be similar between the ^{18}F-FDG and PTF measurements, both in the visual and quantitative analyses.

Use of ^{18}F-FDG and PET is often considered the best approach for myocardial viability assessment. This is largely attributed to the clear contrast of the ^{18}F-FDG accumulation in the myocardium, particularly during the insulin clamp condition, and further due to the high sensitivity of the PET device as compared with the conventional SPECT camera. The accurate image reconstruction of PET technique including the attenuation correction by means of the transmission scan and the significantly smaller contribution of scatter are regarded as other reasons.

It should, however, be noted that the absolute glucose consumption was variable in the normal segment as shown in Figs. 3 and 4. This suggests that the myocardial ^{18}F-FDG uptake is not maximized even during the insulin clamp condition. Previous studies also demonstrated that the glucose uptake is influenced by several physiological factors [26], even during the hyperinsulinemic condition [27]. Thus, accuracy in the viability assessment appeared to be poorer with the absolute measurement of myocardial ^{18}F-FDG uptake as compared with the relative uptake (see Figs. 5, 6; Table 4), as has already been reported by Knuuti

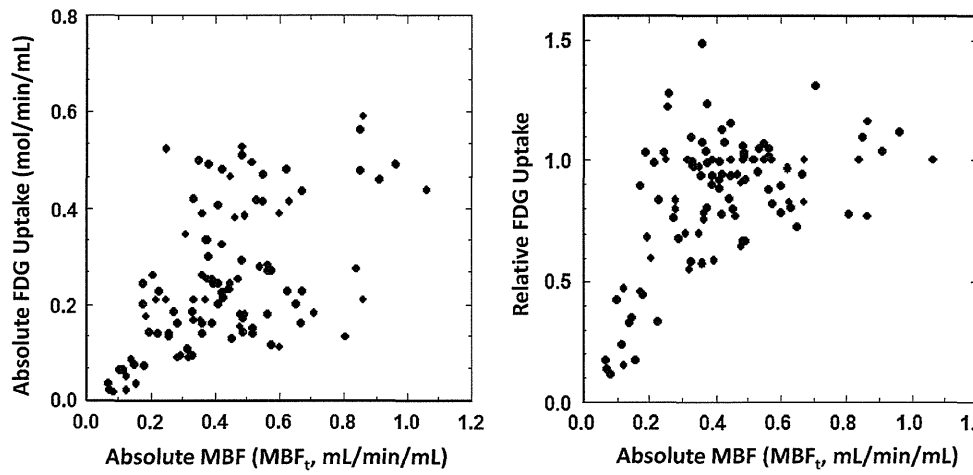

Fig. 3 Relation between ^{18}F-FDG uptake and absolute myocardial blood flow determined by means of ^{15}O-water PET. *Left*: absolute uptake of ^{18}F-FDG which was calculated using the arterial input function. *Right*: relative uptake of ^{18}F-FDG to a control region. MBF_t denotes ml of blood per minutes per ml of regions-of-interest adopted to this plot

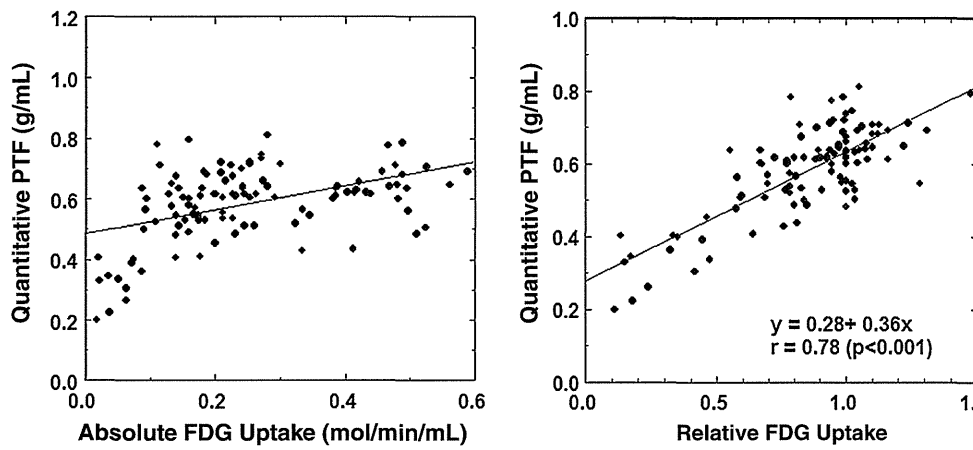

Fig. 4 Relation between the water-perfusable tissue fraction (PTF, g/ml) versus ^{18}F-FDG uptake (*Left*: absolute ^{18}F-FDG uptake. *Right*: relative ^{18}F-FDG uptake)

Table 4 Results of quantitative analysis in terms of evaluating wall motion recovery

Images	Sensitivity (%)	Specificity (%)	PPV (%)	NPV (%)	Accuracy (%)
^{18}F-FDG uptake (relative)	94	75	86	88	87
^{18}F-FDG uptake (absolute)	76	85	90	68	80
Quantitative MBF	68	90	92	62	76
Quantitative PTF	91	85	91	85	89
Quantitative MBF_t	82	90	93	75	85
Glucose (relative) + MBF	97	85	92	94	93

Upper values correspond to only dysfunctional segments, and lower to total segments

et al. [28]. Use of relative uptake of ^{18}F-FDG (or glucose) normalized to a control segment in each subject was therefore suggested for the assessment of myocardial viability. However, the normalization procedure requires a definition of a control segment, which is sometimes subjective and might become a critical procedure, particularly in patients with multiple vessel disease.

The present study showed that the accuracy to predict the functional outcome was improved (the best among the comparisons) when the ^{18}F-FDG was combined with perfusion imaging (Table 4). This was probably attributable to the presence of sub-endocardial scars, which might have been assigned as viable because of increased accumulation of ^{18}F-FDG in the residual tissue (due to the variation). The addition of MBF to PTF is of interest. However, due to the limited number of subjects, further systematic studies are needed with larger number of subjects.

^{15}O-water perfusable-tissue fraction

^{15}O-water is a diffusible and chemically inert tracer [29]. The early distribution after the administration of ^{15}O-water

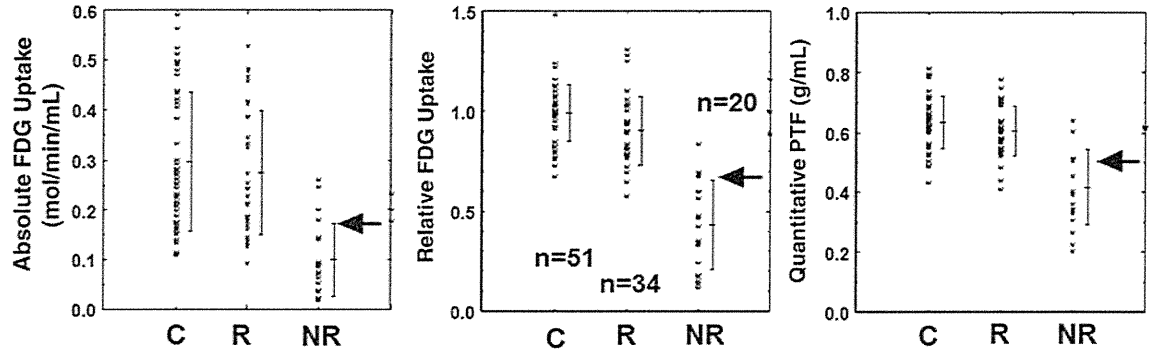

Fig. 5 Absolute and relative ^{18}F-FDG uptake and water-perfusable tissue fraction (PTF) in control segments (C) and in revascularized segments. *Arrows* correspond to the threshold values to discriminate between the recovered (R) and non-recovered (NR) (see text)

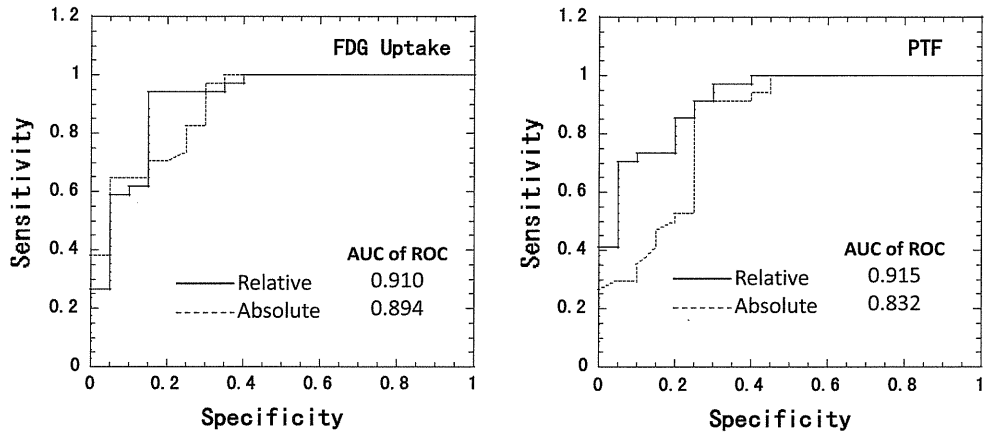

Fig. 6 ROC analysis for wall motion recovery after successful coronary artery bypass graft surgery in patients with hypocontractile function

reflects the regional blood flow [24, 30]. On the other hand, rapid clearance from high flow areas and further uptake into low flow areas cause the myocardial ^{15}O-water distribution, after a sufficient long period, to be proportional to the tissue distribution which is perfused by water [10]. The PTF value estimated from the kinetic ^{15}O-water PET data should represent quantitatively the density of tissue that is capable of rapidly exchanging water within the PET study period. It is hypothesized that the PTF corresponds to the amount of the reversibly injured myocardium in the region of hypocontractile function. This hypothesis is close to the one made for the ^{18}F-FDG PET study, in which the glucose consumption is nearly maximized during the hyperinsulinemic euglycemic condition, so that ^{18}F-FDG accumulation highlights only the myocardial tissue that is not infarcted. Consistency between the two approaches, found in this study, suggests the validity of these hypotheses for both techniques.

In the visual analysis, we observed that the size of the defect in the ^{15}O-water washout phase (qualitative PTF) image was significantly less, and the defect score was smaller than that of ^{18}F-FDG (Table 2). Therefore, the most accurate predictive values were obtained when only the completely normal segments were considered to be viable with the qualitative PTF image, while both normal and mild defects were assigned to be viable with ^{18}F-FDG. Also the quantitative PTF values had significant offsets as compared with ^{18}F-FDG in regions of myocardial infarction (Fig. 4, right). The reason for these is not clear, but is possibly due to the diffusion of ^{15}O-water from the perfusable tissue into the scar regions, or reduced ^{18}F-FDG uptake at the border region close to the scar tissue. Despite this difference, the predictive values for the wall motion recovery were almost equal in both the visual and quantitative analyses.

There are some practical advantages in the PTF and/or PTI approaches for the viability assessment as compared with ^{18}F-FDG. Rapid kinetics of ^{15}O-water allows a short scan, which has the logistical advantage of increasing patient throughput. The short half-life further makes the study repeatable within a short interval, and decreases the radiation dose. The total study duration may be within a half hour including the transmission, ^{15}O-carbonmonoxide and ^{15}O-water scans, if the protocol is optimized [25]. The advent of relatively inexpensive equipment dedicated to the production of ^{15}O-labeled tracers should make this

approach more acceptable to clinical centers. The major limitation of the ^{15}O-water technique was considered as the poor statistics, which is largely due to the short scan period and short half life of ^{15}O. This study, however, demonstrated that information derived from the ^{15}O-water study is essentially consistent with that obtained from the ^{18}F-FDG study. Further development of the image reconstruction technique is highly appreciated to improve the image quality, as has been successfully demonstrated by Katoh et al. [31]. The short half-life also requires the installation of a ^{15}O-dedicated cyclotron in the same facility, as ^{15}O-labeled tracers cannot be delivered from other centers unlike ^{18}F-FDG. There is also concern that the ^{15}O technique is probably sensitive to patient movement during the study, and thus a sophisticated algorithm needs to be developed to correct for any possible movement during the study.

PTF was originally introduced to compensate for the partial volume effect, as a parameter that represents the fractional mass of water-perfusable tissue within the selected ROI. The magnitudes hold the same also for the FDG uptake values, as well as the washout-phase, and the build-up phase images.

In theory, PTF can be affected by heterogeneous flow distribution surrounding the infarction, causing systematic underestimation in PTF [32], as has been demonstrated by Herrero and coworkers [33]. They reported that PTF could be underestimated by as much as 25 % [33], when the tissue contained 4 different flows with minimum flow level >0.10 ml/min/g. However, they also demonstrated in the same report that in the case of a mixture of extremely low flow tissue (e.g., MBF < 0.01 ml/min/g), which should correspond to scar tissue, the estimated PTF values well represented the fraction of only the high flow tissue. Thus, although further investigations will need to include a direct histological and/or histochemical comparison, PTF can still be a reasonable index to represent the fraction of non-scar tissue around the myocardial infarction. The work by Herrero suggested that the perfusion was low enough in the scar tissue to be neglected within the PET examination period.

Limitations of this study

Significant defects were frequently seen in the apical segment in the ^{15}O-water washout image (i.e., the qualitative PTF image). The reason for this may be patient movement during the PET studies, particularly between the ^{15}O-carbonmonoxide and ^{15}O-water scans. This artificial defect was less in the quantitative PTF values, in which values were estimated basically without the ^{15}O-carbonmonoxides blood volume. There were still 4 segments that showed errors in quantitative PTF in the apical region (all below the threshold value) for the wall motion recovery. This was probably due to the smallest thickness and/or the largest wall motion in the apical segment. Note that both PTF and ^{18}F-FDG can be underestimated in the segment in a thin structure and with the wall motion. An independent threshold value may have to be defined for both techniques in this segment.

Future prospects

The ^{15}O-water image at the build-up phase was used as the qualitative MBF image, and the ^{15}O-water washout phase image as the qualitative PTF. This study demonstrated that the washout phase image alone well predicted the wall motion recovery, as accurate as quantitative PTF estimates and ^{18}F-FDG. Recently proposed techniques that calculate the functional images of quantitative MBF and PTF [15, 17, 34] should also be evaluated. Adequacy of such technique including the application of the 3D acquisition should also be evaluated for different PET devices and image reconstruction programs.

No software alignment program was applied in this study, to correct for the possible movement of the patient between the scans. Further study is required to correct for the movement, as has been done in a recent study [35].

It should be noted that the quantitative PTF values and relative ^{18}F-FDG uptake are dependent on the ROI size due to the partial volume effect. For instance, the use of wider ROIs causes a reduction in values. Therefore, the ROI size probably needs to be standardized for each segment. In addition, the reference values and threshold values for viability may need to be defined at each segment.

Conclusion

This study demonstrates that although the image quality is superior with ^{18}F-FDG than with ^{15}O-water, the ^{15}O-water perfusable tissue fraction (PTF) was consistent with the qualitative analysis of ^{18}F-FDG uptake, in terms of the agreement in the defect identification and the assessment of myocardial viability. The image quality is superior with ^{18}F-FDG than with ^{15}O-water, but PTF provided enough information eventually to predict the wall motion recovery after successful revascularization in patients with old myocardial infarction.

Acknowledgments We are greatly indebted to the staff of The Turku PET Center, Turku University Central Hospital, Finland, in particular Mr. Mika Klemetsso and Vesa Oikonen for the computer assistance. We also thank Mr. S. Sekiguchi from Asahi-kasei, co, Tokyo, Japan, for supplying the general-purpose image analysis package, Dr. View. This work was supported by Sigrid Juselius Foundation, Finnish Foundation for Cardiovascular Research, Finland, and a grant from the Ministry of Health, Labour and Welfare (MHLW), Japan.

Conflict of interest None of the authors have any conflict of interest to disclose.

References

1. Rahimtoola SH. A perspective on the three large multicenter randomized clinical trials of coronary bypass surgery for chronic stable angina. Circulation. 1985;72(6 Pt 2):V123–35.
2. Braunwald E, Rutherford JD. Reversible ischemic left ventricular dysfunction: evidence for the "hibernating myocardium". J Am Coll Cardiol. 1986;8(6):1467–70.
3. Rahimtoola SH. The hibernating myocardium. Am Heart J. 1989;117(1):211–21.
4. Marshall RC, Tillisch JH, Phelps ME, et al. Identification and differentiation of resting myocardial ischemia and infarction in man with positron computed tomography, 18F-labeled fluorodeoxyglucose and N-13 ammonia. Circulation. 1983;67(4):766–78.
5. Schwaiger M, Brunken R, Grover-McKay M, et al. Regional myocardial metabolism in patients with acute myocardial infarction assessed by positron emission tomography. J Am Coll Cardiol. 1986;8(4):800–8.
6. Tillisch J, Brunken R, Marshall R, et al. Reversibility of cardiac wall-motion abnormalities predicted by positron tomography. N Engl J Med. 1986;314(14):884–8.
7. Tamaki N, Yonekura Y, Yamashita K, et al. Positron emission tomography using fluorine-18 deoxyglucose in evaluation of coronary artery bypass grafting. Am J Cardiol. 1989;64(14):860–5.
8. Knuuti MJ, Nuutila P, Ruotsalainen U, et al. Euglycemic hyperinsulinemic clamp and oral glucose load in stimulating myocardial glucose utilization during positron emission tomography. J Nucl Med. 1992;33(7):1255–62.
9. Knuuti MJ, Saraste M, Nuutila P, et al. Myocardial viability: fluorine-18-deoxyglucose positron emission tomography in prediction of wall motion recovery after revascularization. Am Heart J. 1994;127(4 Pt 1):785–96.
10. Iida H, Rhodes CG, de Silva R, et al. Myocardial tissue fraction-correction for partial volume effects and measure of tissue viability. J Nucl Med. 1991;32(11):2169–75.
11. Yamamoto Y, de-Silva R, Rhodes CG, et al. A new strategy for the assessment of viable myocardium and regional myocardial blood flow using ^{15}O-water and dynamic positron emission tomography. Circulation. 1992;86(1):167–78.
12. de Silva R, Yamamoto Y, Rhodes CG, et al. Preoperative prediction of the outcome of coronary revascularization using positron emission tomography. Circulation. 1992;86(6):1738–42.
13. Iida H, Tamura Y, Kitamura K, Bloomfield PM, Eberl S, Ono Y. Histochemical correlates of ^{15}O-water-perfusable tissue fraction in experimental canine studies of old myocardial infarction. J Nucl Med. 2000;41(10):1737–45.
14. Teramoto N, Koshino K, Yokoyama I, et al. Experimental pig model of old myocardial infarction with long survival leading to chronic left ventricular dysfunction and remodeling as evaluated by PET. J Nucl Med. 2011;52(5):761–8.
15. Watabe H, Jino H, Kawachi N, et al. Parametric imaging of myocardial blood flow with ^{15}O-water and PET using the basis function method. J Nucl Med. 2005;46(7):1219–24.
16. Harms HJ, de Haan S, Knaapen P, Allaart CP, Lammertsma AA, Lubberink M. Parametric images of myocardial viability using a single 15O–H2O PET/CT scan. J Nucl Med. 2011;52(5):745–9.
17. de Haan S, Harms HJ, Lubberink M, et al. Parametric imaging of myocardial viability using oxygen-15 labelled water and PET/CT: comparison with late gadolinium enhanced CMR. Eur J Nucl Med Mol Imaging. 2012 (in press).
18. Spinks TJ, Araujo LI, Rhodes CG, Hutton BF. Physical aspects of cardiac scanning with a block detector positron tomograph. J Comput Assist Tomogr. 1991;15(5):893–904.
19. DeFronzo RA, Tobin JD, Andres R. Glucose clamp technique: a method for quantifying insulin secretion and resistance. Am J Physiol. 1979;237(3):E214–23.
20. Nuutila P, Koivisto VA, Knuuti J, et al. Glucose-free fatty acid cycle operates in human heart and skeletal muscle in vivo. J Clin Invest. 1992;89(6):1767–74.
21. Iida H, Takahashi A, Tamura Y, Ono Y, Lammertsma AA. Myocardial blood flow: comparison of oxygen-15-water bolus injection, slow infusion and oxygen-15-carbon dioxide slow inhalation. J Nucl Med. 1995;36(1):78–85.
22. Iida H, Rhodes CG, de Silva R, et al. Use of the left ventricular time-activity curve as a noninvasive input function in dynamic oxygen-15-water positron emission tomography. J Nucl Med. 1992;33(9):1669–77.
23. Iida H, Kanno I, Takahashi A, et al. Measurement of absolute myocardial blood flow with $H_2^{15}O$ and dynamic positron-emission tomography. Strategy for quantification in relation to the partial-volume effect. Circulation. 1988;78(1):104–15.
24. Araujo LI, Lammertsma AA, Rhodes CG, et al. Noninvasive quantification of regional myocardial blood flow in coronary artery disease with oxygen-15-labeled carbon dioxide inhalation and positron emission tomography. Circulation. 1991;83(3):875–85.
25. Iida H, Miura S, Shoji Y, et al. Noninvasive quantitation of cerebral blood flow using oxygen-15-water and a dual-PET system. J Nucl Med. 1998;39(10):1789–98.
26. Buxton DB, Schelbert HR. Measurement of regional glucose metabolic rates in reperfused myocardium. Am J Physiol. 1991; 261(6 Pt 2):H2058–68.
27. Maki M, Luotolahti M, Nuutila P, et al. Glucose uptake in the chronically dysfunctional but viable myocardium. Circulation. 1996;93(9):1658–66.
28. Knuuti MJ, Nuutila P, Ruotsalainen U, et al. The value of quantitative analysis of glucose utilization in detection of myocardial viability by PET. J Nucl Med. 1993;34(12):2068–75.
29. Kety SS. The theory and applications of exchange of inert gas at the lungs and tissues. Pharmacol Res. 1951;3:1–41.
30. Bergmann SR, Fox KA, Rand AL, et al. Quantification of regional myocardial blood flow in vivo with $H_2^{15}O$. Circulation. 1984;70(4):724–33.
31. Katoh C, Ruotsalainen U, Laine H, et al. A new iterative reconstruction method based on median root prior in quantification of myocardial blood flow and oxygen metabolism with PET. J Nucl Med. 1999;40(5):862–7.
32. Huang S, Mahoney D, Phelps M. Quantitation in positron emission tomography: 8. Effect of non-linear parameter estimation on functional images. J Comput Assist Tomogr. 1987;11:314–25.
33. Herrero P, Staudenherz A, Walsh JF, Gropler RJ, Bergmann SR. Heterogeneity of myocardial perfusion provides the physiological basis of perfusable tissue index. J Nucl Med. 1995;36(2): 320–7.
34. Harms HJ, Knaapen P, de Haan S, Halbmeijer R, Lammertsma AA, Lubberink M. Automatic generation of absolute myocardial blood flow images using [15O]H2O and a clinical PET/CT scanner. Eur J Nucl Med Mol Imaging. 2011;38(5):930–9.
35. Koshino K, Watabe H, Hasegawa S, Hayashi T, Hatazawa J, Iida H. Development of motion correction technique for cardiac (15)O-water PET study using an optical motion tracking system. Ann Nucl Med. 2009;24(1):1–11.

Koshino et al. EJNMMI Research 2012, 2:33
http://www.ejnmmires.com/content/2/1/33

EJNMMI Research
a SpringerOpen Journal

ORIGINAL RESEARCH Open Access

Breath-hold CT attenuation correction for quantitative cardiac SPECT

Kazuhiro Koshino[1], Kazuhito Fukushima[2], Masaji Fukumoto[2], Kazunari Sasaki[3], Tetsuaki Moriguchi[1], Yuki Hori[1], Tsutomu Zeniya[1], Yoshihiro Nishimura[2], Keisuke Kiso[2] and Hidehiro Iida[1*]

Abstract

Background: Attenuation correction of a single photon emission computed tomography (SPECT) image is possible using computed tomography (CT)-based attenuation maps with hybrid SPECT/CT. CT attenuation maps acquired during breath holding can be misaligned with SPECT, generating artifacts in the reconstructed images. The purpose of this study was to investigate the effects of respiratory phase during breath-hold CT acquisition on attenuation correction of cardiac SPECT imaging.

Methods: A series of ^{201}Tl-emission and ^{99m}Tc-based transmission computed tomography (TCT) scans was carried out along with CT-attenuation scans on 11 young normal volunteers using a hybrid SPECT/CT scanner. The CT scans were performed at three respiratory phases: end-inspiration (INS), end-expiration (EXP), and the midpoint (MID) between these phases. Using alignment parameters between attenuation maps and SPECT images without attenuation or scatter corrections, quantitative SPECT images were reconstructed, including corrections for attenuation and scatter. Regional radioactivity concentrations normalized by the subjects' weights were compared between CT- and TCT-based attenuation correction techniques.

Results: SPECT images with CT attenuation maps at the EXP phase showed significant differences in regional weight-normalized radioactivity concentrations relative to the images using the other attenuation maps ($p < 0.05$), as well as systematic positive bias errors, compared to TCT-based images for all myocardial segments, 5.7% ± 2.7% (1.9% to 10.0%). No significant differences in regional weight-normalized radioactivity concentrations were observed between images with CT attenuation maps at MID and INS phases or between these and the TCT-based images, but regional tendencies were found: for anterior to anterolateral segment, positive bias of 5.0% ± 2.2% (1.3% to 8.1%) and 5.6% ± 1.9% (2.6% to 8.5%) and for inferior to inferoseptal segment, negative bias of −5.3% ± 2.6% (−9.1% to −1.7%) and −4.6% ± 2.5% (−8.8% to −1.5%) for the MID and INS phases, respectively.

Conclusions: Use of breath-hold CT attenuation maps at INS and MID phases for attenuation and scatter corrections demonstrated accurate quantitative images that would prove beneficial in cardiac SPECT/CT studies.

Background

Single photon emission computed tomography (SPECT) has the unique ability to provide functional images of biological tissues *in vivo*. As is the case with positron emission tomography (PET), corrections for attenuation and scatter are important. Previous studies have demonstrated improvements in diagnostic accuracy when applying corrections for both attenuation and scatter [1]. Attenuation correction has been widely carried out by means of transmission computed tomography (TCT) scanning, with several mechanical configurations such as rotating rod sources fitted with parallel-beam collimator systems, and a single rod source placed at the focal line of a symmetrical fan-beam collimator [2-4]. It has been demonstrated that TCT data can also be used for scatter correction [5], and that when coupled with kinetic analysis, the overall accuracy of reconstructed SPECT images is sufficiently high for quantitation of various physiological functions in the thoracic region [6-8] and also in the brain [9]. Several dedicated TCT systems developed by various manufacturers have resulted in improved diagnostic accuracy. It has also been reported

* Correspondence: iida.hidehiro.ri@mail.ncvc.go.jp
[1]Department of Investigative Radiology, National Cerebral and Cardiovascular Center Research Institute, 5-7-1 Fujishirodai, Suita, Osaka 565-8565, Japan
Full list of author information is available at the end of the article

that when using optimally designed TCT equipment, reconstructed images are accurate and applicable to quantitative studies in the thoracic region [10].

Myocardial blood flow (MBF) quantitation has been shown to be feasible using ^{201}Tl and dynamic SPECT if proper procedures are applied to accurately correct for attenuation and scatter [8]. It has been demonstrated that a kinetic modeling approach can be applied to quantitatively obtained SPECT data to determine regional myocardial blood flow. In fact, in a canine study with correction for all necessary factors, MBF values assessed at rest, after beta-blocker administration, and during adenosine infusion were in good agreement with those determined in a microsphere experiment [11]. Based on these previous works, it is likely that correction for attenuation and scatter is an important key for the establishment of absolute MBF measurement in cardiac SPECT.

Recently, an X-ray computed tomography (CT)-based method of attenuation correction has been implemented with commercial PET cameras and now has become standard as a combined PET/CT system. This type of system has been used primarily not only in oncology studies but also for the quantitation of myocardial perfusion using ^{13}N-ammonia [12]. Combination of multislice CT and SPECT systems has been shown to result in accurate reconstruction in myocardial studies [13]. A problem, however, has been noted when applying CT information to attenuation correction in the thoracic region. Erroneous observations occur and are attributed to misregistration between CT and PET images. These are associated not only with global patient movement but also with respiratory motion. Previously, ^{68}Ge-based TCT scans were carried out for 3 to 10 min at each bed position and, thus, provided spatially and temporally smoothed images that were consistent with the emission data, resulting in no systematic artifacts in reconstructed PET images. On the other hand, the CT-based method, which provides frozen images during one respiratory phase, can cause significant mismatches with PET data and, thus, cause artifacts, often in the apex and lateral wall regions [14].

The same problem has also been noted with combined SPECT/CT systems [15,16]. These studies recommended careful review of attenuation correction maps as well as software-based re-registration in order to avoid reconstruction artifacts due to misregistration.

In cardiac studies with PET/CT, it would be ideal to match cine CT to PET images at each phase [17] or to use respiratory-averaged CT information as the attenuation map for reconstructing single-frame PET data sets [18]. However, these techniques require large radiation doses for multiple CT scans, resulting in their limited use in clinical studies. In contrast, it has been noted that the use of CT images acquired at specific phases provides reasonable accuracy in producing attenuation-corrected PET images [18].

The purpose of this study was to investigate the effect of respiratory phase on breath-hold CT-based attenuation correction (CT-AC) for quantitative cardiac SPECT imaging. The CT-based attenuation maps were acquired from normal volunteers at three respiratory phases: end-inspiration (INS), end-expiration (EXP), and the midpoint (MID) between these phases. The attenuation maps were used for quantitative SPECT (QSPECT, National Cerebral and Cardiovascular Center and QSPECT group, Japan), namely for scatter correction using transmission-dependent convolution subtraction technique followed by ordered-subset expectation maximization (OSEM) reconstruction with attenuation correction [8,19]. The CT-corrected emission images were compared with images reconstructed using ^{99m}Tc TCT-based attenuation maps, which have been validated in a previous article [10].

Methods

Subjects

Subjects consisted of 11 healthy volunteers (7 men, 4 women; age range, 18 to 25 years; mean age ± SD, 21.4 ± 2.3 years; mean weight ± SD, 55.4 ± 5.2 kg). The volunteers had no signs or symptoms of ischemic heart disease. The study protocol was approved by the ethics committee of the National Cerebral and Cardiovascular Center. Prior to the scan, all subjects gave written informed consent for participation in this study.

Image acquisition

All subjects were placed in supine position with arms up and scanned at rest using a hybrid SPECT/CT scanner, the Symbia T6 (Siemens, Knoxville, TN, USA). As shown

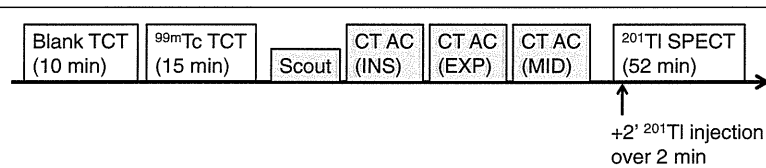

Figure 1 Protocol for cardiac SPECT/CT and ^{99m}Tc TCT. INS, EXP, and MID denote respiratory phases at end-inspiration, end-expiration, and the midpoint between these phases, respectively.

in Figure 1, the study protocol consisted of ^{99m}Tc-based blank and TCT scans, X-ray CT scans, and a dynamic SPECT.

A 10-min blank scan and a 15-min TCT scan, used as references for CT-AC, were performed using a TCT system validated in a previous work [10]. A small scatter fraction with maximum sensitivity was achieved by optimizing the collimator gap for the ^{99m}Tc source. The system was attached to an opposing two-headed detector with low-energy, high-resolution (LEHR) collimators, as shown in Figure 2A. The TCT source consisted of a 3-m long tube (5 mm in diameter) filled with 740 MBq of ^{99m}Tc, which was equivalent to seven separate rod sources. Each rod was collimated axially with lead sheets. The TCT system was removed from the SPECT detector before the following scans.

After acquisition of a CT scout image, breath-hold CT-AC scans were performed at the INS, EXP, and MID respiratory phases. CT acquisition parameters were as follows: helical scan time, 10 s; rotation cycle, 1 s; pitch, 1.0; tube voltage, 130 kVp; tube current, 100 mA over 10 s; slice thickness, 5 mm; slice interval, 5 mm; matrix size, 512×512; pixel size, 0.98×0.98 mm^2; and maximum duration for holding breath, 16 s. For breath-hold CT acquisition at each phase, a system of monitoring and displaying respiratory phase was introduced. Briefly, a subject's abdominal respiratory motion was determined using an optical motion-tracking device, POLARIS (Northern Digital Inc., Ontario, Canada), to monitor the location of an infrared-reflective target placed on the abdominal surface, as shown in Figure 2B,C. The accuracy of the device was 0.35-mm root mean square (RMS), as reported by the manufacturer. The motion was displayed on a screen using an ellipsoidal indicator to enable the subject to control his or her own breathing in real time. The subject breathed deeply several times to determine the marker's range of motion between the EXP and INS phases before the CT-AC scans. The MID phase was defined as occurring when the marker was located at the central position of the motion range.

Dynamic SPECT begun 2 min before the start of the 2-min constant infusion of 111-MBq ^{201}Tl. Projection data were acquired using the detector heads positioned opposing each other (H-mode) with the LEHR collimators in continuous mode and in a circular orbit because QSPECT reconstruction was performed on geometric-mean projections. The frame collection rates and 360° rotation times were 6×2 min (28 s) and 8×5 min (148 s); number of views, degrees per view, matrix size, and enlargement factor were 45 views, 4° per view, 64×64, and 1.45, respectively. A 34% energy window centered on 77 keV was used for the ^{201}Tl acquisitions [7,20].

Image reconstruction

SPECT projection data were processed to generate a quantitative image, that is, pixel values were calibrated in Bq/mL. The procedure was as follows: (1) TCT projections normalized by blank projections and CT projections were reconstructed and then linearly scaled to provide attenuation maps for ^{201}Tl. For CT images, filtering to SPECT spatial resolution using the B08s filter, which was called by the manufacturer, interpolation to equate the matrix and pixel sizes to those of TCT attenuation map, and conversion from Hounsfield units to attenuation coefficients were performed using Syngo MI Application, version 7.0.7.14 (Siemens, Knoxville, TN, USA). (2) A SPECT image was temporarily reconstructed using a filtered backprojection algorithm without scatter or attenuation correction. Each attenuation map was manually aligned to the SPECT image using translations along three orthogonal directions by interactively moving the attenuation map image over the SPECT image. The interactive fusion was performed using the QSPECT software package. The overlap in the aligned images was assessed in coronal, sagittal, and

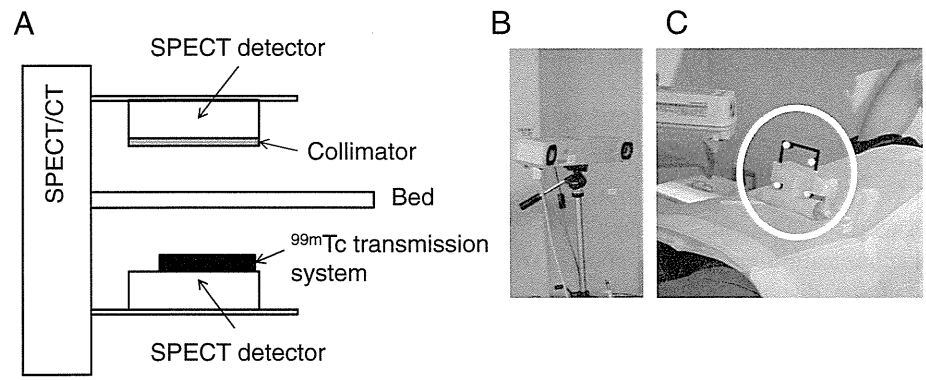

Figure 2 Experimental setup. (**A**) Schematic diagram of ^{99m}Tc transmission system attached to a SPECT/CT detector. (**B**) and (**C**) System to monitor respiratory motion; (B) optical motion-tracking device. (C) Infrared-reflective target placed on the subject's abdominal surface.

transaxial views based on the distances of myocardial contours between the anterior to lateral regions of the attenuation map and the SPECT images. (3) Using each alignment parameter, scatter- and attenuation-corrected images were reconstructed with OSEM (three iterations, five subsets using geometric-mean projections, post-reconstruction Gaussian filter of 7.0 mm in full width at half maximum) provided by the QSPECT software package [8], respectively.

Data analysis

Each dynamic image reconstructed using the four attenuation maps was summed into a static image with the 14.5- to 34.5-min frames (mid-scan time). Transformation to a short-axis orientation was based on a static image corrected with a TCT attenuation map (TCT-AC image). The transformation was also applied to the static images corrected with CT attenuation maps (CT-AC images). The radioactivity concentrations of the images were normalized by the subject's weight. Variability of normalized radioactivity concentrations in the myocardium was also assessed. Polar maps for the left ventricles were generated from the static images. In this process, the basal slice and apical region were defined on the TCT-AC image. The definition was also used for the CT-AC images of the same subject. In addition, percent differences between the weight-normalized radioactivity concentrations of TCT-AC and CT-AC images were calculated as $100 \times \frac{CT-TCT}{TCT}$. Regional radioactivity concentration values and percent differences were evaluated for myocardial segments by dividing polar maps into 17 segments according to the AHA 17-segment model [21]. To evaluate the effects of attenuation correction with the four attenuation maps on SPECT images, the regional radioactivity of TCT-AC and CT-AC images was statistically tested using the Tukey multiple comparisons method. Homogeneity of radioactivity distribution among the 17 myocardial segments was also assessed using the Tukey multiple comparisons method for each dataset of TCT-AC and CT-AC images. A p-value of less than 0.05 was considered statistically significant.

Results

Breath-hold CT-AC scans at three respiratory phases were performed successfully for all subjects. The amplitude of the marker indicating respiratory phases, which was defined as half the distance between the infrared-reflective targets at the INS and EXP phases, was 8.50 ± 5.58 (2.51 to 17.50) mm. Translations to align attenuation maps to SPECT image was listed in Table 1. Cephalad/caudal translations were dominant among three orthogonal directions, especially in CT attenuation maps at the MID and the EXP phases. Figure 3 shows examples of TCT and CT attenuation map images at the three phases. In coronal and sagittal views at the INS phase, the surfaces of the inferior regions of the myocardium and the liver were clearly separated. On the other hand, at the EXP phase, it was difficult to distinguish these surfaces. The position of the heart relative to the liver at the MID phase seemed to be similar to that of

Table 1 Translations to align attenuation maps to SPECT image (mean ± SD)

Attenuation map	Direction		
	Right/left (mm)	Up/down (mm)	Cephalad/caudal (mm)
TCT	0.0 ± 0.0	0.0 ± 0.0	2.4 ± 2.1
CT at MID	2.8 ± 7.1	−2.6 ± 3.9	11.7 ± 8.0
CT at INS	4.5 ± 6.0	−4.7 ± 5.4	6.2 ± 7.3
CT at EXP	−1.5 ± 3.5	0.0 ± 5.1	19.9 ± 5.8

CT, computed tomography; EXP, end-expiration; INS, end-inspiration; MID, midpoint; TCT, transmission computed tomography.

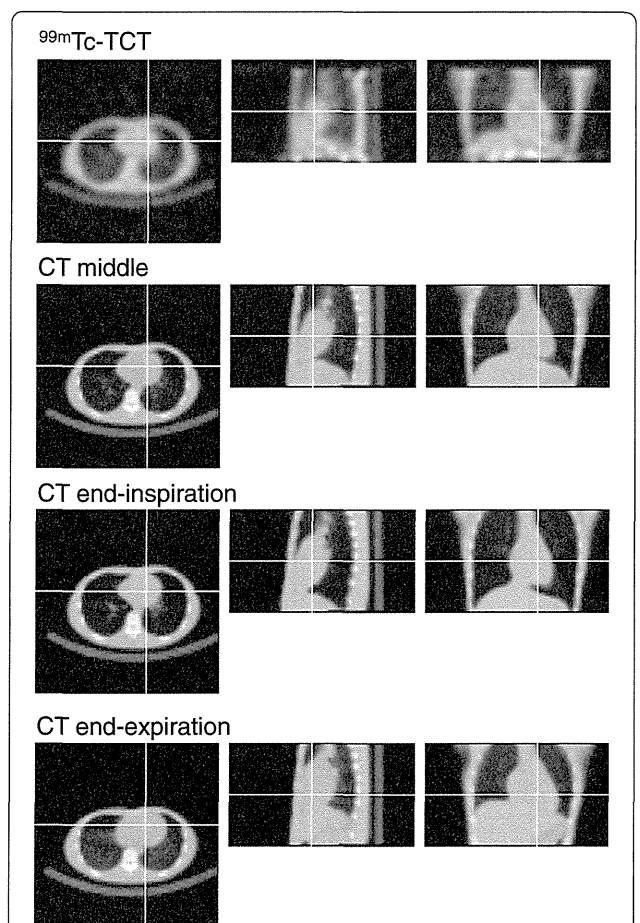

Figure 3 Attenuation map images of ^{99m}Tc-TCT and CT at three different respiratory phases. The left, middle, and right columns represent transaxial, sagittal, and coronal views, respectively.

TCT attenuation map rather than those at the other respiratory phases. Figure 4 shows SPECT images for the same subject as Figure 3. The left, middle, and right columns represent slices at basal, middle, and apical levels, respectively.

The distribution of weight-normalized radioactivity concentration and the differences between TCT-AC and CT-AC images are shown in Figure 5. The left column displays polar maps of averaged radioactivity concentration, normalized using the maximum value of the TCT-AC map. Statistical analysis of the SPECT image datasets with the four attenuation maps indicated that the images corrected with EXP attenuation maps were different significantly from the other datasets, that is, significant differences in weight-normalized radioactivity concentrations were observed between TCT-EXP, INS-EXP, and MID-EXP image datasets (there was no significant difference in weight-normalized radioactivity concentration between TCT-INS, TCT-MID, and INS-MID). No regional differences were found in weight-normalized radioactivity concentrations of any datasets, although relatively large values in inferior regions were observed for all TCT-AC and CT-AC image datasets. As shown in the right column, the polar map of the percent difference for CT-AC images of EXP phases shows a positive bias, 5.7% ± 2.7% (1.9% to 10.0%), over all segments. Regional tendencies were found for CT-AC images of the other two phases: for the anterior to anterolateral segments, positive biases of 5.0% ± 2.2% (1.3% to 8.1%) and 5.6% ± 1.9% (2.6% to 8.5%) and for the inferior to inferoseptal segments, negative biases of −5.3% ± 2.6% (−9.1% to −1.7%) and −4.6% ± 2.5% (−8.8% to −1.5%) for the MID and INS phases, respectively. The worst segmental percent differences (mean ± SD and the worst individual value) were 10.5% ± 4.9%, 22.6% in the basal inferolateral segment for the EXP phase; −4.8% ± 4.8%, −11.0% and −8.0% ± 6.4%, −18.4% in the mid inferior segments for the MID and the INS phases, respectively. The percent difference excluding the worst

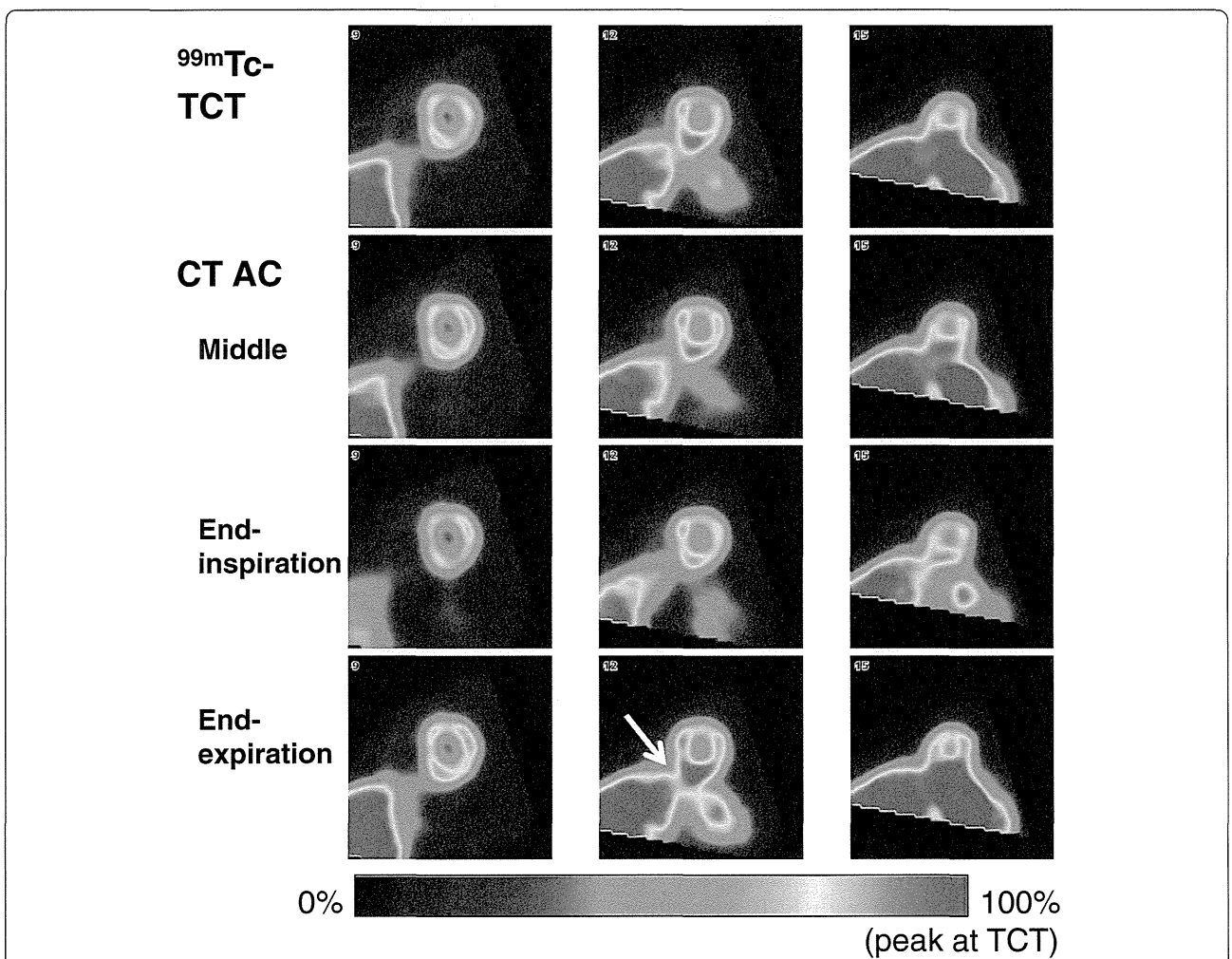

Figure 4 SPECT images corrected for attenuation and scatter using TCT and CT attenuation maps. The left, middle, and right columns represent slices at the basal, middle, and apical levels, respectively. The subject was the same as in Figure 3.